Synchronization of semiconductor lasers with complex dynamics within a multi-nodal network

Michail Bourmpos, Apostolos Argyris and Dimitris Syvridis

National and Kapodistrian University of Athens, Panepistimiopolis, Ilisia, 15784, Greece
E-mail: mmpour@di.uoa.gr , argiris@di.uoa.gr , dsyvridi@di.uoa.gr

Abstract: Semiconductor lasers are non-linear devices that exhibit stable, periodic, complex or chaotic dynamics, and in coupled configurations - under strict conditions - can be efficiently synchronized. Applications in communications using such devices for increased security usually employ a twofold system, the emitter and the receiver. In this investigation we examine the potential of this synchronization property to extend to communication networks with as many as 50 or 100 users (nodes) that are coupled to each other through a central node, in a star network topology.
Keywords: Chaos synchronization, mutual coupling, network synchronization, semiconductor lasers.

1. Introduction

Over the past decades a lot of effort has been put into exploiting chaotic dynamics of signals in areas like communications [1-3], control systems [4], artificial intelligence [5] and more. Chaotic signals emitted from semiconductor lasers (SLs) have been frequently used in security applications for data encryption [6], random number generation [7] etc. A usual configuration that the above types of applications employ consists of two elements - the emitter and the receiver - whose outputs are efficiently synchronized. More complex configurations have been adopted in recent works, where the idea of building a network of coupled SLs emitting synchronized chaotic signals has been proposed [8]. More specifically, Fischer et al [9] have demonstrated isochronal synchronization between two SLs relayed through a third SL, even in cases of large coupling time delays. Zamora-Munt et al [10] have shown operation in synchrony of 50 to 100 distant lasers, coupled through a central SL in a star network topology. In the above work, couplings between distant lasers and the central one are symmetric and the time delays (distances) from the central to the star lasers are assumed equal. The optical injection effect is based on moderate coupling strengths while little attention has been paid on the complexity and the spectral distribution of the signals.

In our work we use a large population -50 to 100- distant lasers which proves to be a sufficient number for good synchrony of the optical signals emitted, as discussed in [10]. Strong optical injection and asymmetric mutual couplings are adopted, enabling the increase on the effect that lasers have to each other through mutual coupling, while preserving the level of output optical power in

logic values (up to a few mW). Although intrinsic laser characteristics are selected to be identical in our simulations, different laser operational frequencies were assumed in terms of detuning values from a reference frequency $_{0}$.

2. Network Architecture and Rate Equations

We first consider a star network topology with $=50$ semiconductor lasers, which from now on we will refer to as 'star lasers', relayed through a central similar semiconductor laser, called 'hub laser'.
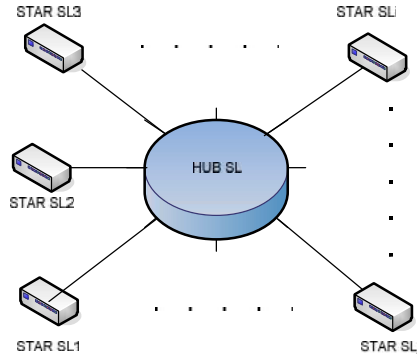

Figure 1. Star network architecture of N 'star' lasers, relayed through mutual couplings with a central 'hub' laser

A rate equation mathematical model is used to describe the operation and dynamics of the above system of devices. This model is based on the Lang Kobayashi rate equation model [11], originating from the representation used in [9] and including frequency detuning terms as in [10]. The complex optical fields and carrier numbers for the star and hub lasers can be calculated from:

$$\frac{dE_j(t)}{dt} = i\Delta\omega_j E_j(t) + \frac{1}{2}(1+ia)\left(G_j(t) - \frac{1}{t_{ph}}\right)E_j(t) + k_H E_H(t-\tau_H)$$
$$+ \sqrt{D}\xi_j(t)$$

$$\frac{dN_j(t)}{dt} = \frac{I_j}{e} - \frac{N_j(t)}{t_s} - G_j(t)|E_j(t)|^2$$

$$\frac{dE_H(t)}{dt} = i\Delta\omega_H E_H(t) + \frac{1}{2}(1+ia)\left(G_H(t) - \frac{1}{t_{ph}}\right)E_H(t) + \beta \cdot \sum_{j=1}^{N} k_j E_j$$
$$+ \sqrt{D}\xi_H(t)$$

$$\frac{dN_H(t)}{dt} = \frac{I_H}{e} - \frac{N_H(t)}{t_s} - G_H(t)|E_H(t)|^2$$

$$G_{j,H}(t) = \frac{g_n(N_{j,H}(t) - N_0)}{1 + s|E_{j,H}(t)|^2}$$

All laser have identical intrinsic parameters, with values as follows:

TABLE 1
INTRINSIC LASER PARAMETERS

	linewidth enhancement factor	5
t_{ph}	photon lifetime	$2 psec$
$_0$	reference laser frequency	$2 \cdot \cdot _0$
$_0$	reference laser wavelength	$1550 nm$
D	noise strength	$10^{-5} nsec^{-1}$
e	electronic charge	$1.602 \cdot 10^{-19}$ C
t_s	carrier lifetime	$1.54 nsec$
g_n	gain coefficient	$1.2 \cdot 10^{-5} nsec^{-1}$
N_0	carrier density at transparency	$1.25 \cdot 10^8$
s	gain saturation coefficient	$5 \cdot 10^{-7}$

$_j(t)$ and $_H(t)$ are uncorrelated complex Gaussian white noises for the star and hub lasers respectively. The star lasers are biased at $I_j=25$mA, while the hub laser is biased at $I_H=9$mA, well below the solitary lasing threshold ($I_{th}=17.4$mA). Each laser is detuned with respect to the reference laser frequency $_0$, at variable values $_j$ (star lasers) and $_H$ (hub laser). Especially for the hub laser detuning, we can assume $_H=0$ without loss of generality. Delay times ($_j=_H=5$ns) and coupling strengths $k_j=k_H=k$ are identical. Coupling asymmetry is achieved through the asymmetry coupling coefficient . While each star laser receives a single injection field from the hub (k_H), the hub laser receives the sum of injection fields (k_j) of the *N* star lasers, which could be rather large. To counteract for this large value, receives values smaller than 1, decreasing the overall injected optical field into the hub, keeping it within a realistic range of values.

3. Simulations and Numerical Results

Simulations were performed for the set of rate equations presented, using the 4th order Runge-Kutta method, with a time-step of 0.8psec. Optical power is deducted from the complex optical field using the appropriate conversion [12]. First we have evaluated the behavior of N=50 star lasers with detuning values ±1GHz around the reference frequency, following a Gaussian distribution, for different values of coupling strength and coupling asymmetry coefficient. Star lasers are ordered based on their detuning, so the 1st laser has the most negative detuning, while the 50th has the largest positive one. Based on these simulations, a mapping of mean and minimum zero-lag cross-correlation between the 50 star lasers was built. As we can see in figure 2, two different yellow-white areas of high correlation exist, one for low and one for high values of the product of coupling strength and coupling asymmetry coefficient ($k \cdot$).

Moving along the diagonal from lower left to upper right corner of figure 2(i) - that is from lower to higher values of the product $k \cdot$ - we encounter the

following areas: first a small area in black, where correlation is low, the star lasers operate in CW mode with noise and the hub is not receiving enough coupling in order to emit in lasing mode.
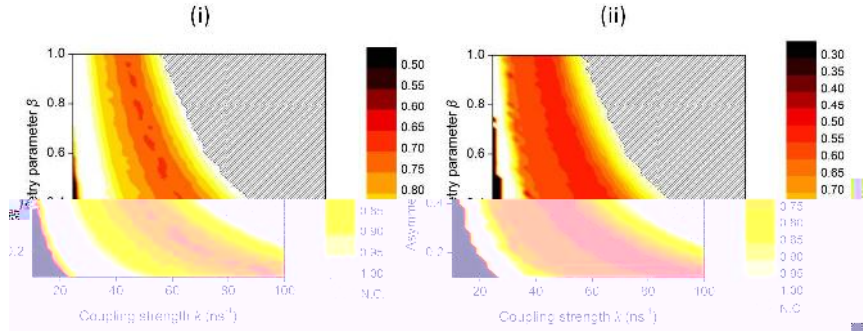

Figure 2. Mean (i) and minimum (ii) zero-lag correlation for 50 lasers with ±1GHz detuning values

Then we come across a white area, where $k \cdot$ product has small values; the star lasers are characterized with periodic dynamics and the hub laser emits just above threshold. A further increase of $k \cdot$ leads to star laser emission with chaotic dynamics (yellow-orange area). The hub laser now emits in the order of few hundreds μW but the mean correlation experiences significant decrease. As the product $k \cdot$ increases optical injection becomes large enough to drive the star lasers into emitting signals of high correlation (small yellow-white stripe). The complexity of these signals slightly decreases and the hub laser now emits in the order of several mW. Finally the hatched area is an uncharted region where optical injection and emitted optical powers are unrealistically large and the rate equation model does not converge.
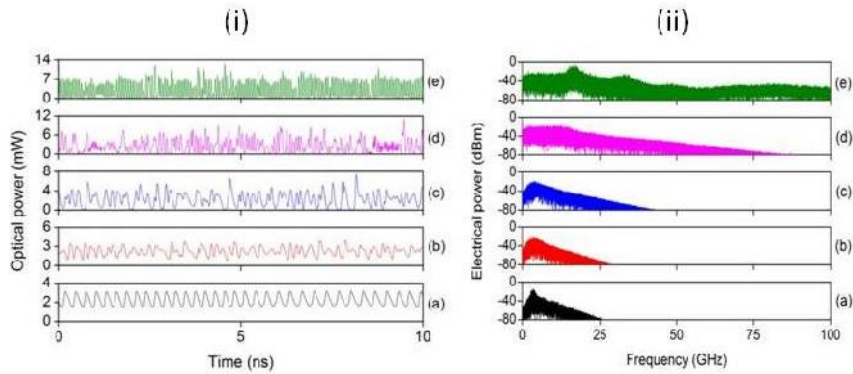

Figure 3 Time traces (i) and spectra (ii) of a single laser for network of 50 lasers with ±1GHz detuning values, coupling strengths $k_j = k_H = 60nsec^{-1}$ and coupling asymmetry coefficients (a) =0.15, (b) =0.2, (c) =0.4, (d) =0.8 and (e) =1.

Time traces and spectra of the different cases we have just described are shown in figure 3(ii), for a fixed coupling strength value of $k=60nsec^{-1}$. It is evident that for larger values of the product $k·$ we have faster oscillations attributed to bandwidth enhancement, as has been commonly reported in cases of strong optical injection [13-14].
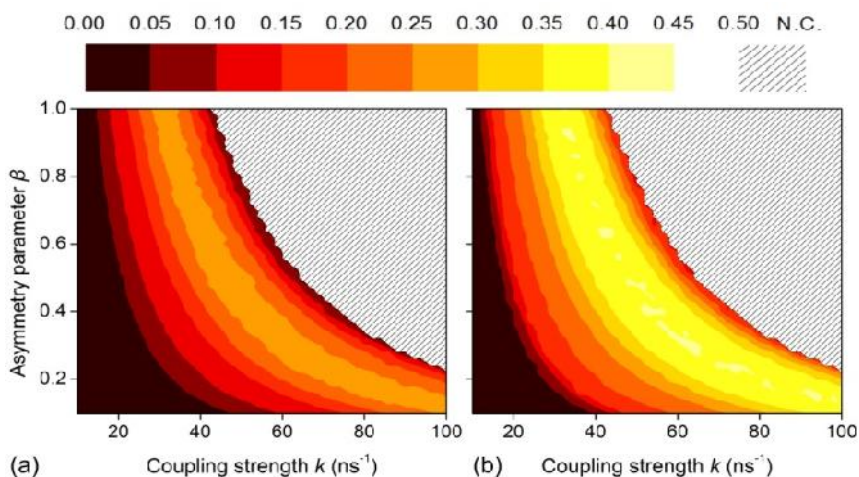

Figure 4. Mean (a) and maximum (b) synchronization error for 50 lasers with ±1GHz detuning values

Another useful parameter we have estimated to evaluate the star lasers output waveforms is the zero-lag synchronization error. Synchronization error is normalized in the mean value of the ith and jth laser, averaged in the duration T_{av} and is thus expressed in the form:

$$\varepsilon_{ij} = \langle \frac{\left| P_i(t) - P_j(t) \right|}{0.5 \cdot \left(P_i(t) + P_j(t) \right)} \rangle \qquad (6)$$

As expected, small values of synchronization error between the ith and j[th] laser are achieved in the same areas where good zero-lag cross-correlation exists (figure 4 vs figure 2). Based on figure 4 we can identify (k,) pairs where the maximum synchronization error, which indicates the worst behavior in our network, is minimal. One such pair is $k=60nsec^{-1}$, =0.5. For this case of parameters we depict the zero-lag correlation between the ith and j[th] laser (figure 5i). The worst case of synchronization - in which we encounter the minimum correlation - occurs for the pair of lasers with the far most frequency detuning, that is between lasers 1 and 50. We can also observe that lasers with similar detuning values have good correlations with respect to each other, even when possessing large absolute detuning values.

The superimposed time traces of the 50 star lasers for the above pair of parameters are shown in figure 5(ii). We can observe highly synchronized signals at zero lag for the biggest part of the time window depicted.

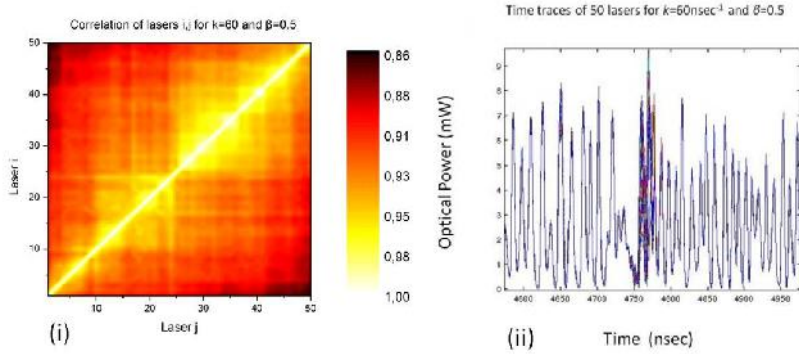However we can identify small periods of time where synchronization may be lost.

Figure 5. (i) Zero-lag correlation between 50 lasers with ±1GHz detuning values, coupling strengths $k_j=k_H=60$nsec^{-1} and coupling asymmetry coefficient =0.5.
(ii) Time traces of 50 superimposed star laser outputs ±1GHz detuning values, for he parameter pair $k=60$nsec^{-1}, =0.5

The star lasers rapidly synchronize again after a few ns. This phenomenon is repeated in the complete time series and is mainly responsible for the synchronization error calculated, since the synchronization error in the rest of the time window is almost zero.

By increasing the frequency detuning range of the star lasers from ±1GHz to ±10GHz, the system necessitates much larger values of the product $k\cdot$ in order to force the hub laser into lasing emission (figure 6i). As a result, the first area examined, where the star lasers emit in CW mode, is enlarged. The area of non-convergence remains almost the same, while areas of complex dynamics and large cross-correlation values are minimized.

To counteract the increase in the detuning values we attempt to increase the number of star lasers in the network from N=50 to N=100. It is apparent in figure 6ii that inserting more lasers in the network leads to more optical power injected in the hub laser, which now emits for smaller values of the product $k\cdot$. However, small increase in the areas of good cross-correlation is observed.
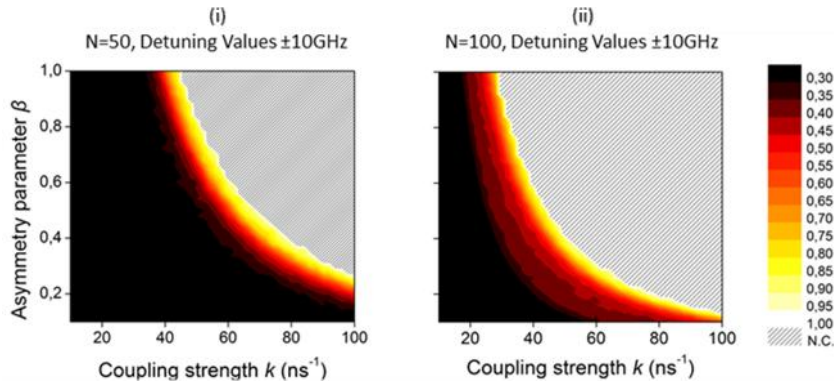
Figure 6. Mean zero-lag correlation for (i) N=50 and (ii) N=100 lasers
with ±10GHz detuning values

Another attempt to counteract the increase in detuning values is to lower the
pump current of the star lasers to I=18mA near the lasing threshold. This
reduces the effect the star lasers dynamics have in the network. In figure 7 we
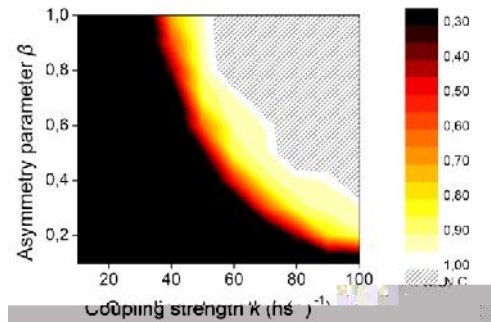can observe significant increase of the areas of good cross-correlation.

Figure 7. Mean zero-lag correlation for N=50 and pump current I=18mA for the
star lasers

Finally, a small analysis was carried out on the type of synchronization
occurring in the network and the role the hub laser plays on it. Figure 8 clearly
shows that the hub lasers dynamics lag behind the dynamics of the star lasers by
exactly the time delay between star and hub lasers, that is $\tau_{j} = \tau_{H} = 5$ns. As a
deduction we can say that the hub laser holds a passive role in the network,
operating solely as a relay between the star lasers. The internal parameters of the
star lasers, the time delay, coupling strength, asymmetry and driving current
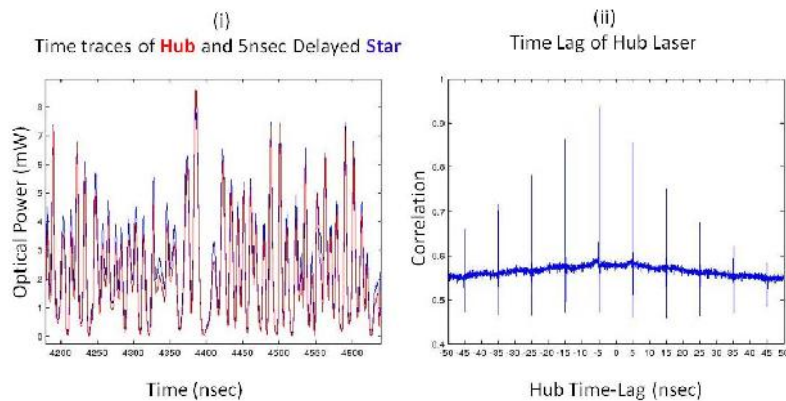seem to be solely responsible for the dynamics of the system.

Figure 8. (i) Time traces of hub(red) and one random star (blue) delayed by

5nsec lasers, (ii) Cross-correlation time lag of hub and one random star laser

4. Conclusions

A star network topology with multiple nodes consisting of typical semiconductor lasers has been presented and investigated. Two general areas of good synchronization have been identified, each one with different characteristics in terms of dynamics. The first one, for small values of total optical injection ($k\cdot$ product), produces optical signals of simpler dynamics, while the second one, for large values of $k\cdot$, produces signals with high complexity dynamics. An increase in the number of nodes in the network has proved to enlarge these areas and provide synchronization improvement.

References

[1]   L.M. Pecora and T.L. Caroll, "Synchronization in chaotic systems," *Phys. Rev. Lett.*, vol. 64, 821-824, 1990.

[2]   P. Colet and R. Roy, "Digital communication with synchronized chaotic lasers," *Opt. Lett.*, vol. 19, pp. 2056–2058, 1994.

[3]   A. Argyris, D. Syvridis , L. Larger, V. Annovazzi-Lodi, P. Colet, I. Fischer, J. García-Ojalvo, C.R. Mirasso, L. Pesquera and K.A. Shore, "Chaos-based communications at high bit rates using commercial fiber-optic links," *Nature*, vol. 438, n. 7066, pp. 343-346, 2005.

[4]   A.L. Fradkov, R.J. Evans and B.R. Andrievsky, "Control of chaos: methods and applications in mechanics," *Phil. Trans. R. Soc. A*, vol. 364, 2279-2307, 2006.

[5]   C. R. Mirasso, P. Colet, and P. Garcia-Fernandez, "Synchronization of chaotic semiconductor lasers: Application to encoded communications," *IEEE Photon. Technol. Lett.,* vol. 8, pp. 299–301, 1996.

[6]   V. Annovazzi-Lodi, S. Donati, and A. Scire, "Synchronization of chaotic injected laser systems and its application to optical cryptography," *IEEE J. Quantum Electron.*, vol. 32, pp. 953–959, 1996.

[7]   A. Uchida, K. Amano, M. Inoue, K. Hirano, S. Naito, H. Someya, I. Oowada, T. Kurashige, M. Shiki, S. Yoshimori, K. Yoshimura, and P. Davis, "Fast physical random bit generation with chaotic semiconductor lasers", Nature Photon. 2, 728–732 (2008).

[8]   R. Vicente, I. Fischer, and C. R. Mirasso, "Synchronization properties of three-coupled semiconductor lasers," *Phys. Rev. E*, vol. 78, 066202, 2008.

[9]   I. Fischer, R. Vicente, J.M. Buldú, M. Peil, C.R. Mirasso, M.C. Torrent and J. García-Ojalvo, "Zero-Lag Long-Range Synchronization via Dynamical Relaying," *Phys. Rev. Lett.*, vol. 97, 123902, 2006.

[10] J. Zamora-Munt, C. Masoller, J. Garcia-Ojalvo and R. Roy "Crowd synchrony and quorum sensing in delay-coupled lasers," *Phys. Rev. Lett.*, vol. 105, 264101, 2010.

[11] R. Lang and K. Kobayashi, "External optical feedback effects on semiconductor injection laser properties," *IEEE J. Quantum Electron.*, vol. 16, pp. 347-355, 1980.

[12] K. Petermann, *Laser Diode Modulation And Noise*, New Ed. Kluwer Academic Publishers Group (Netherlands), 1991.

[13] T.B. Simpson and J.M. Liu and A. Gavrielides, "Bandwidth enhancement and broadband noise reduction in injection-locked semiconductor lasers," *IEEE Photon. Technol. Lett.*, vol. 7, pp. 709-711, 1995.

[14]   A. Murakami, K. Kawashima and K. Atsuki, "Cavity resonance shift and bandwidth enhancement in semiconductor lasers with strong light injection," *IEEE Quantum Electron.*, vol.39, pp. 1196-1204, 2003.